Third-Harmonic Generation in Photonic Topological Metasurfaces

Daria Smirnova,[1,2] Sergey Kruk,[1] Daniel Leykam,[3] Elizaveta Melik-Gaykazyan,[1,4] Duk-Yong Choi,[5] and Yuri Kivshar[1]

[1]*Nonlinear Physics Centre, Australian National University, Canberra ACT 2601, Australia*
[2]*Institute of Applied Physics, Russian Academy of Science, Nizhny Novgorod 603950, Russia*
[3]*Center for Theoretical Physics of Complex Systems, Institute for Basic Science (IBS), Daejeon 34126, Republic of Korea*
[4]*Faculty of Physics, Lomonosov Moscow State University, Moscow 119991, Russia*
[5]*Laser Physics Centre, Australian National University, Canberra ACT 2601, Australia*

We study nonlinear effects in two-dimensional photonic metasurfaces supporting topologically protected helical edge states at the nanoscale. We observe strong third-harmonic generation mediated by optical nonlinearities boosted by multipolar Mie resonances of silicon nanoparticles. Variation of the pump-beam wavelength enables independent high-contrast imaging of either bulk modes or spin-momentum-locked edge states. We demonstrate topology-driven tunable localization of the generated harmonic fields and map the pseudospin-dependent unidirectional waveguiding of the edge states bypassing sharp corners. Our observations establish dielectric metasurfaces as a promising platform for the robust generation and transport of photons in topological photonic nanostructures.

Topological photonics describes optical structures with the properties analogous to electronic topological insulators [1]. These systems are distinguished by bulk band gaps that host disorder-robust states localized at edges or interfaces and provide a novel approach for designing nonreciprocal or localized modes for optical isolators, photonic-crystal waveguides, and lasers. Since the original demonstration of backscattering-immune photonic topological edge states with the use of a gyrotropic microwave photonic crystal under a strong magnetic field [2], there has been a concerted effort toward realizing topological photonics at the nanoscale. Recently suggested optical designs compatible with nonmagnetic all-dielectric structures [3–8] are now emerging as a promising platform for quantum and nonlinear topological photonics [9–12].

Stimulated by the progress in nanofabrication techniques, a new favorable ground for topological photonics based on dielectric nanoparticles with high refractive index has recently emerged [13,14]. Strong optical resonances and low Ohmic losses make it feasible for practical implementation of topological order for light at subwavelength scales. The underlying conceptual framework is to use arrays of meta-atoms with judiciously engineered shape and lattice structure, with topologically nontrivial features arising from pseudo-spin degrees of freedom. It bridges fundamental physics of topological phases with resonant nanophotonics and multipolar electrodynamics [15,16]. Topological metasurfaces could form a ground for a new class of ultrathin devices with functionalities based on novel physical principles through engineering light-matter interactions in synthetic photonic potentials [17]. Their pseudospin-dependent physics may be useful for manipulation of internal degrees of freedom of light such as polarization and angular momentum.

However, the experimental characterization of topological photonic structures becomes much more challenging at the nanoscale. Most implementations so far have been limited to *indirect probing* of topological states such as transmission spectra [11,18–20], which cannot provide spatially resolved information about the edge modes and suffer from input or output coupling losses. Other recently demonstrated linear approaches such as near-field imaging [21], cathodoluminescence [22], and far-field imaging [23] suffer from poor spatial resolution or small field of view, leaving the edge states almost completely hidden in the background noise. Direct high-contrast imaging of the edge states is essential for assessing the fidelity of the topological waveguides and for optimizing the coupling with localized emitters [5].

Here we show that nonlinear topological photonics provides an effective way to overcome these limitations by observing nonlinear light conversion in a topological photonic nanostructure. By varying the frequency and polarization of a pump beam and measuring the generated third-harmonic signal, we demonstrate selective imaging of either bulk modes or edge modes that are otherwise undetectable via conventional linear far field imaging. Our approach significantly enhances the measurement contrast, sensitivity, and imaging area compared to other recent works, enabling us to unambiguously visualize nanoscale topological photonic edge states and their propagation around corners and defects. Importantly, our platform combining appreciably strong optical nonlinearity with topological band structures paves the way toward observing other nonlinear wave interactions in photonic topological insulators.
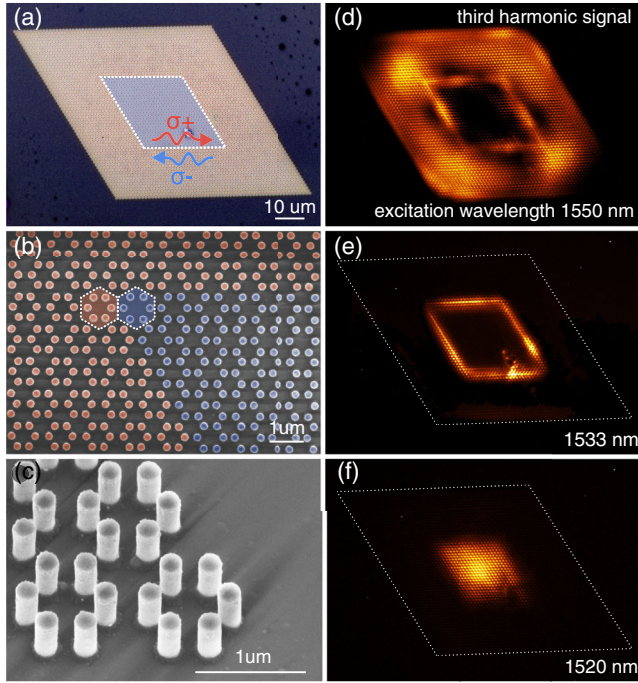
FIG. 1. Experimental results for dielectric metasurfaces with topological edge states. (a) Optical microscope image of a topological metasurface guiding robust edge waves with opposite helicities ($\sigma^{\pm}$) along the interface between topologically different outer and inner domains (painted blue). Dashed line—guide for a eye. (b),(c) Scanning electron microscopy images: (b) top view and (c) side view of the metasurface consisting of silicon pillars arranged into hexagon clusters. (b) Domain wall between expanded (blue) and shrunken (red) domains. Framed hexagons highlight corresponding unit cells. Pillars' radius $r = 105$ nm, height $h = 538$ nm, lattice constant of hexagon clusters $a = 1100$ nm, shrink or expand coefficients are 0.95 and 1.05, correspondingly. (d)–(f) Experimental images of third-harmonic intensity distribution for three excitation wavelengths.

For our experiments, we design photonic all-dielectric metasurfaces exhibiting a topological phase transition and band inversion above the light line, similar to an earlier theoretical proposal [3]. The array of silicon nanopillars hexamers is divided into two domains—expanded or shrunken hexamers—characterized by distinct topological invariants. Their interface supports a pair of topologically protected, spin-momentum locked edge states [3,18,24,25].

We fabricate our samples from silicon on a glass substrate (for details, see the Supplemental Material [26]). Figures 1(a)–1(c) show optical and electron microscope images of one of the fabricated samples, consisting of a rhomboid-shaped domain of expanded hexamers embedded in a domain of shrunken hexamers. We illuminate the sample with a powerful short-pulse laser with a tunable wavelength [35]; see details in [26]. The laser beam size is larger than the total size of the sample. The strong cubic nonlinearity of silicon [27,36] naturally

provides optical frequency conversion capabilities, and the resonant near-field enhancement provided either by bulk or edge modes boosts the nonlinear harmonic generation [16], enabling accurate mapping of the corresponding modes. The generated third-harmonic (TH) radiation is imaged on a camera; see [26].

Figures 1(d)–1(f) show three representative cases of the TH distribution at different pump frequencies: in Figs. 1(d) and 1(f), the TH comes from the bulk of the shrunken or expanded regions. This corresponds to resonant excitation of bulk dipolar modes in these two domains. In Fig. 1(e), the pump is tuned to the bulk band gap of the two domains, and the TH signal is generated along the domain wall between the shrunken and expanded structures, visualizing the topological edge states. We notice that in our experiments the coupling to the edge states at normal incidence is inefficient, and the result presented in Fig. 1(e) is an average of two images obtained at $\pm 1°$ incident angles. Within the band gap frequency range, resonant excitation of high-quality topological edge states induces tightly localized nonlinear light sources with magnitudes strongly exceeding nonlinear response in the bulk. In Fig. 1(e), the experimentally measured TH intensity at the topological domain wall is 3 orders of magnitude higher than the TH intensity coming from the bulk (see details in Fig. S4 of the Supplemental Material [26]).

To demonstrate the potential of the nonlinear diagnostics technique, we additionally perform sets of complimentary *linear measurements* for identical experimental configurations with the results presented in [26]. With linear approach we are able to observe convincingly the excitation of bulk modes, although with a substantially degraded signal-to-noise ratio. However, the topological light localization along the domain wall remains invisible in our linear experiments (see discussions and the results of linear measurements in Sec. II of [26]). It is vastly easier to observe edge states using the conventional linear imaging in the large-scale designs of topological systems based on the waveguide geometry [37], with a typical size of the building blocks much larger than the wavelength of light. But linear imaging becomes increasingly difficult with nanoscale platforms compatible with planar silicon-based integrated optics.

To explain the wavelength-dependent optical response and the observed edges states, we model each nanopillar as an out-of-plane dipole with predominant E_z component of the electric field directed along the vertical axis. The collective modes supported by the individual hexamers can be classified according to their in-plane symmetry, with the bands in the spectral range of interest composed primarily of dipole (p) and quadrupole (d) hexamer eigenmodes. In the vicinity of the Γ point, the bulk photonic band structure is captured by the eigenvalue problem $\mathcal{E}|\psi_{\pm}\rangle = \hat{H}_{\pm}|\psi_{\pm}\rangle$, with the effective Hamiltonian forming 2×2 blocks $\hat{H}_{\pm}$ given by
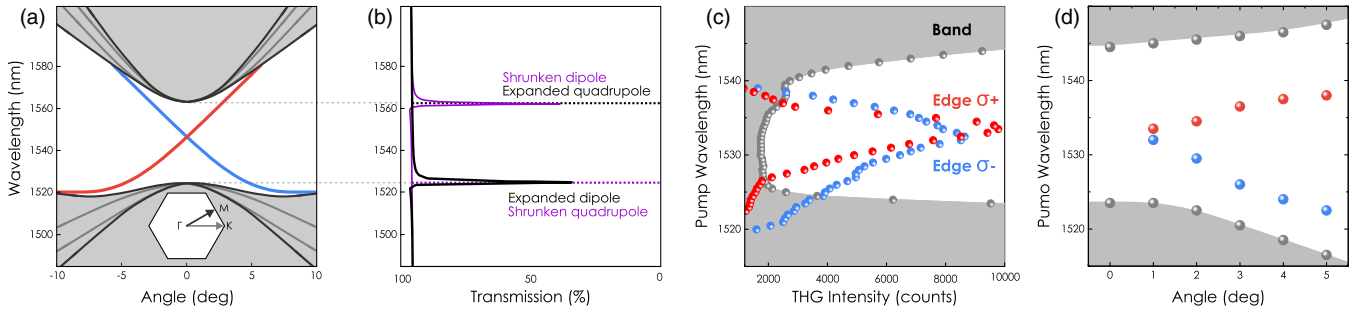
FIG. 2. Dispersion properties of the topological helical edge states. (a) Numerically calculated photonic band structures for the four doublet bands along $\Gamma - M$ (black curves) and $\Gamma - K$ (dark gray curves) directions, found almost perfectly overlaid for shrunken and expanded arrays. The bulk bands are shaded in light gray, while the dispersion branches of the edge modes spanning the topological band gap are shown by colored curves. Inset: Brillouin zone. (b) Simulated transmission spectra of the infinite expanded and shrunken metasurfaces featuring excitation of dipolar resonances at normal incidence. Note that the optical response of the fabricated sample is spectrally blue shifted by approximately 15 nm. (c) Experimentally measured TH spectrum indicating the mid-gap edge states excited at the interfaces of the rhomboid topological cavity. (d) Spectral positions of TH maxima depending on angle of incidence trace diverging dispersion branches for opposite circular polarizations.

$$\hat{H}_{\pm} = \begin{pmatrix} \mu + \beta k^2 & v(\mp k_x - ik_y) \\ v(\mp k_x + ik_y) & -\mu - \beta k^2 \end{pmatrix}, \quad (1)$$

corresponding to the two circular polarizations of eigenstates $|\psi_{\pm}\rangle = (|p_{\pm}\rangle, |d_{\pm}\rangle)^T$ [18]. Equation (1) incorporates effective parameters: μ and β are the mass term and band parabolicity, respectively, v is velocity; $k_{x,y}$ are in-plane components of the wave vector. The two decoupled polarizations form a pseudospin degree of freedom and thus the spin Chern number $C = (C_- - C_+)/2$ can be introduced, where $C_{\pm}$ is Chern number for each individual block [28]. Each of the blocks in Eq. (1) has the structure of a Dirac-like Hamiltonian, for which the spin Chern number can be straightforwardly calculated as $C = \frac{1}{2}(\text{sgn}\mu - \text{sgn}\beta)$ [28]. The shrunken domain is described by the condition $\mu\beta > 0$ ($C = 0$; trivial), whereas the condition $\mu\beta < 0$ is valid for the expanded domain ($C = 1$; nontrivial), in accordance with Ref. [3]; thus, the interface states are topologically protected. The edge states bound to the interface $x = 0$ exhibit linear dispersion crossing $\mathcal{E}_{\text{e.s.}}(k_y) = \pm v k_y$.

Figure 2(a) shows the numerically computed bulk band diagram of the structure (for details of numerical simulations, see [26]). The bulk modes are primarily quadrupolar or dipolar, and the transition from shrunken to expanded designs is accompanied by a band inversion. At the normal incidence, the external radiation can only couple to the dipolar modes, as seen in the calculated transmission spectra in Fig. 2(b). When the pump is tuned to the upper band edge, it is resonant only with the dipolar bulk modes of the shrunken outer domain, whereas at the lower band edge it is resonant with the dipolar bulk modes of the expanded inner domain. Hence, the localization of nonlinear light generation occurs, as the wavelength is varied mapping the band inversion.

Figure 2(a) additionally illustrates the characteristic Dirac-like dispersion of the spin-momentum locked edge states

residing in the band gap, which can be selectively excited using a circularly polarized pump beam. Figure 2(c) shows the experimental TH spectra for 1° incidence measured from the bulk (gray dots) and from the domain wall excited with the two orthogonal circular polarizations of the pump laser beam (red and blue). The two polarizations excite the edge modes with the opposite helicity values σ^+ and σ^-.

We experimentally measure the dispersion of the edge states by tilting the sample along its horizontal axis between $0°$ and $5°$ and tracing the maxima of the TH spectra [see Fig. 2(d)]. Since our domain wall forms a closed cavity, to distinguish between the σ^+ and σ^- states we sample the TH intensity from the upper part of the domain wall only (on the lower edge their dispersion is opposite). Figure 2(d) shows the spectral separation of the σ^+ and σ^- states as the angle increases. In particular, their dispersion is close to linear, indicating the edge states are nearly gapless and decoupled, consistent with their topological origin.
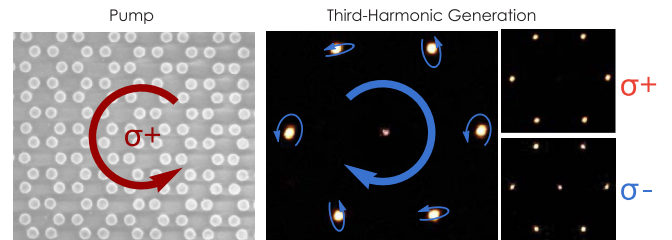

FIG. 3. Nonlinear diffraction and polarization conversion. Experimentally observed back-focal plane images of the TH signal generated by an all-dielectric metasurface consisted of an inner domain of shrunken hexamers and outer domain of expanded hexamers in the forward direction for the left-handed circularly polarized pump, σ^+, at 0° incident angle for the fundamental wavelength of 1540 nm which corresponds to a bulk state. Blue arrows visualize the polarization state of the TH fields. Right: back-focal plane patterns of the TH field for two states of an analyzer: left-handed (top) and right-handed (bottom) circular polarized.
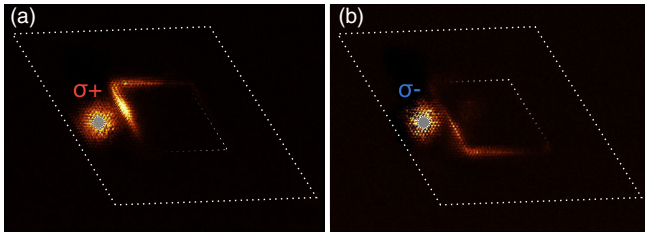
FIG. 4. Spin-momentum-locked topological guided modes. Experimental images of the third-harmonic intensity distribution for the pump focused within the dashed circle with (a) left-circular and (b) right-circular polarizations.

Nonlinear diffraction from the metasurface sample exhibits a characteristic hexagonal far-field pattern. It is accompanied by the circular polarization conversion due to the nonlinear interference of the induced multipolar sources related to the excited photonic modes of the metasurface (see Secs. IV and VI of [26]). We perform the polarimetry [29] of the third-harmonic signal and observe the polarization conversion of σ^+ pump into σ^- harmonic and vice verse in the zeroth diffraction order, as summarized in Fig. 3. The nonlinear conversion efficiency is estimated to be comparable to the efficiency of previously demonstrated silicon Mie-resonant metasurfaces [16,30,31]; see details in Sec. III of [26].

Next, we study the spin-momentum-locked waveguiding of the optical edge modes associated with the analogue of the quantum spin Hall effect for light [3,32–34,38]. In this design, the edge states are topologically protected by the C_{6v} rotational symmetry of the hexamers [3]. As long as this symmetry is preserved, the counter-propagating edge states remain decoupled and cannot scatter backward, even when the interface has sharp corners, as in our system. To excite and map the counter-propagating edge modes individually, we locally focus the circularly polarized pump beam in a spot near the domain wall [see the dashed circle in Figs. 4(a) and 4(b)]. In Fig. 4(a), the pump with σ^+ polarization couples to the mode propagating clockwise, while in Fig. 4(b) the σ^- pump launches the counterclockwise wave propagation. Both waves propagate along the domain wall passing the corners.

Finally, we demonstrate the existence of the edge states for arbitrary geometries of the topological interfaces. For this, we fabricate a metasurface with a domain wall similar to the shape of the Australian continent; see Fig. 5. When the whole metasurface is pumped with the wavelength corresponding to that of the edge mode, the domain wall becomes clearly imaged via the third-harmonic field contour.

Beyond imaging, nanofabricated topological photonic cavities of arbitrary geometries may be employed as nonlinear light sources for efficient converting infrared radiation to visible light, with tunability of near and far field characteristics governed by the topological band inversion, and intrinsic protection against fabrication imperfections. This
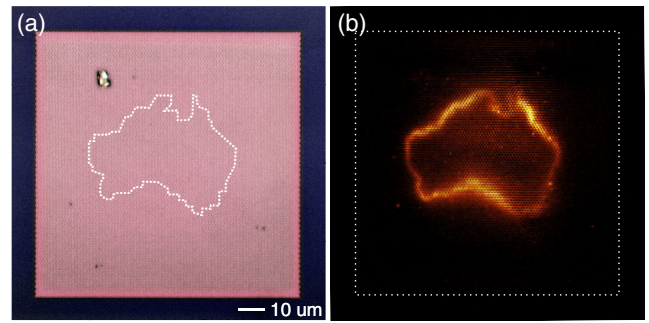

FIG. 5. Topological Australia: an example of a third-harmonic image generated from geometry-independent edge states. (a) Optical microscope image of a metasurface with a domain wall of a shape of the Australian continent. Dashed line is a guide for an eye for the domain wall between the shrunken and the expanded domains. (b) Experimentally observed third-harmonic field at the edge-state pump wavelength.

opens prospects for singular optics and frequency mixing driven by topological effects. For example, in Sec. X of [26] we simulate the conversion of orbital angular momentum using helical edge states excited at a closed edge contour with sharp corners.

In summary, we have suggested and demonstrated a novel approach for imaging topological edge states with third-harmonic generation. Compared to linear imaging, our nonlinear approach offers superior contrast, sensitivity, and large imaging area, enabling both characterization and optimization of topological waveguides for applications. We have observed pseudospin-momentum locking of edge photonic modes at the topological interfaces, verifying their ability to propagate around sharp corners. Furthermore, we have demonstrated tunable localization and enhanced harmonic generation in topological photonic structures. Our results help bridge nonlinear optics with topological physics for the integrated and robust photonic circuitry at the nanoscale.

[1] L. Lu, J. D. Joannopoulos, and M. Soljačić, Topological states in photonic systems, Nat. Phys. 12, 626 (2016).
[2] Z. Wang, Y. Chong, J. D. Joannopoulos, and M. Soljačić, Observation of unidirectional backscattering-immune

topological electromagnetic states, Nature (London) **461,** 772 (2009).

[3] L.-H. Wu and X. Hu, Scheme for Achieving a Topological Photonic Crystal by Using Dielectric Material, Phys. Rev. Lett. **114,** 223901 (2015).

[4] A. Slobozhanyuk, S. H. Mousavi, X. Ni, D. Smirnova, Y. S. Kivshar, and A. B. Khanikaev, Three-dimensional all-dielectric photonic topological insulator, Nat. Photonics **11,** 130 (2017).

[5] T. Ma and G. Shvets, All-Si valley-Hall photonic topological insulator, New J. Phys. **18,** 025012 (2016).

[6] S. Barik, H. Miyake, W. DeGottardi, E. Waks, and M. Hafezi, Two-dimensionally confined topological edge states in photonic crystals, New J. Phys. **18,** 113013 (2016).

[7] P. D. Anderson and G. Subramania, Unidirectional edge states in topological honeycomb-lattice membrane photonic crystals, Opt. Express **25,** 23293 (2017).

[8] M. I. Shalaev, W. Walasik, A. Tsukernik, Y. Xu, and N. M. Litchinitser, Robust topologically protected transport in photonic crystals at telecommunication wavelengths, Nat. Nanotechnol. **14,** 31 (2019).

[9] B. Bahari, A. Ndao, F. Vallini, A. El Amili, Y. Fainman, and B. Kanté, Nonreciprocal lasing in topological cavities of arbitrary geometries, Science **358,** 636 (2017).

[10] M. A. Bandres, S. Wittek, G. Harari, M. Parto, J. Ren, M. Segev, D. N. Christodoulides, and M. Khajavikhan, Topological insulator laser: Experiments, Science **359,** eaar4005 (2018).

[11] S. Barik, A. Karasahin, C. Flower, T. Cai, H. Miyake, W. DeGottardi, M. Hafezi, and E. Waks, A topological quantum optics interface, Science **359,** 666 (2018).

[12] S. Mittal, E. A. Goldschmidt, and M. Hafezi, A topological source of quantum light, Nature (London) **561,** 502 (2018).

[13] A. I. Kuznetsov, A. E. Miroshnichenko, M. L. Brongersma, Y. S. Kivshar, and B. Luk'yanchuk, Optically resonant dielectric nanostructures, Science **354,** aag2472 (2016).

[14] M. S. Rider, S. J. Palmer, S. R. Pocock, X. Xiao, P. A. Huidobro, and V. Giannini, A perspective on topological nanophotonics: Current status and future challenges, J. Appl. Phys. **125,** 120901 (2019).

[15] D. A. Smirnova, A. B. Khanikaev, L. A. Smirnov, and Y. S. Kivshar, Multipolar third-harmonic generation driven by optically induced magnetic resonances, ACS Photonics **3,** 1468 (2016).

[16] D. Smirnova and Y. S. Kivshar, Multipolar nonlinear nanophotonics, Optica **3,** 1241 (2016).

[17] X. Ni, D. Purtseladze, D. A. Smirnova, A. Slobozhanyuk, A. Alù, and A. B. Khanikaev, Spin- and valley-polarized one-way klein tunneling in photonic topological insulators, Sci. Adv. **4,** eaap8802 (2018).

[18] M. A. Gorlach, X. Ni, D. A. Smirnova, D. Korobkin, D. Zhirihin, A. P. Slobozhanyuk, P. A. Belov, A. Alù, and A. B. Khanikaev, Far-field probing of leaky topological states in all-dielectric metasurfaces, Nat. Commun. **9,** 909 (2018).

[19] M. I. Shalaev, S. Desnavi, W. Walasik, and N. M. Litchinitser, Reconfigurable topological photonic crystal, New J. Phys. **20,** 023040 (2018).

[20] X.-T. He, E.-T. Liang, J.-J. Yuan, H.-Y. Qiu, X.-D. Chen, F.-L. Zhao, and J.-W. Dong, A silicon-on-insulator slab for topological valley transport, Nat. Commun. **10,** 872 (2019).

[21] S. Kruk, A. Slobozhanyuk, D. Denkova, A. Poddubny, I. Kravchenko, A. Miroshnichenko, D. Neshev, and Y. Kivshar, Edge states and topological phase transitions in chains of dielectric nanoparticles, Small **13,** 1603190 (2017).

[22] S. Peng, N. J. Schilder, X. Ni, J. van de Groep, M. L. Brongersma, A. Alù, A. B. Khanikaev, H. A. Atwater, and A. Polman, Probing the Band Structure of Topological Silicon Photonic Lattices in the Visible Spectrum, Phys. Rev. Lett. **122,** 117401 (2019).

[23] N. Parappurath, F. Alpeggiani, L. Kuipers, and E. Verhagen, Direct observation of topological edge states in silicon photonic crystals: Spin, dispersion, and chiral routing, arXiv:1811.10739.

[24] S. Yves, R. Fleury, T. Berthelot, M. Fink, F. Lemoult, and G. Lerosey, Crystalline metamaterials for topological properties at subwavelength scales, Nat. Commun. **8,** 16023 (2017).

[25] J. Noh, W. A. Benalcazar, S. Huang, M. J. Collins, K. P. Chen, T. L. Hughes, and M. C. Rechtsman, Topological protection of photonic mid-gap defect modes, Nat. Photonics **12,** 408 (2018).

[26] See Supplemental Material at http://link.aps.org/supplemental/10.1103/PhysRevLett.123.103901 for detailed descriptions of the optical characterization, theoretical models, multipolar analysis, and full-wave numerical simulations of the nonlinear response in topological metasurfaces, which includes Refs. [3,15,16,18,27–34].

[27] X. Gai, D.-Y. Choi, and B. Luther-Davies, Negligible nonlinear absorption in hydrogenated amorphous silicon at 1.55 μm for ultra-fast nonlinear signal processing, Opt. Express **22,** 9948 (2014).

[28] S.-Q. Shen, *Topological Insulators. Dirac Equation in Condensed Matters* (Springer, New York, 2012).

[29] S. S. Kruk, M. Decker, I. Staude, S. Schlecht, M. Greppmair, D. N. Neshev, and Y. S. Kivshar, Spin-polarized photon emission by resonant multipolar nanoantennas, ACS Photonics **1,** 1218 (2014).

[30] S. Kruk and Y. Kivshar, Functional meta-optics and nanophotonics governed by Mie resonances, ACS Photonics **4,** 2638 (2017).

[31] M. R. Shcherbakov, D. N. Neshev, B. Hopkins, A. S. Shorokhov, I. Staude, E. V. Melik-Gaykazyan, M. Decker, A. A. Ezhov, A. E. Miroshnichenko, I. Brener, A. A. Fedyanin, and Y. S. Kivshar, Enhanced third-harmonic generation in silicon nanoparticles driven by magnetic response, Nano Lett. **14,** 6488 (2014).

[32] B. A. Bernevig, T. L. Hughes, and S.-C. Zhang, Quantum spin Hall effect and topological phase transition in HgTe quantum wells, Science **314,** 1757 (2006).

[33] P. Michetti, P. H. Penteado, J. C. Egues, and P. Recher, Helical edge states in multiple topological mass domains, Semicond. Sci. Technol. **27,** 124007 (2012).

[34] K. Y. Bliokh, D. Smirnova, and F. Nori, Quantum spin Hall effect of light, Science **348,** 1448 (2015).

[35] L. Wang, S. Kruk, K. Koshelev, I. Kravchenko, B. Luther-Davies, and Y. Kivshar, Nonlinear wavefront control with all-dielectric metasurfaces, Nano Lett. **18,** 3978 (2018).

[36] A. S. Shorokhov, E. V. Melik-Gaykazyan, D. A. Smirnova, B. Hopkins, K. E. Chong, D.-Y. Choi, M. R. Shcherbakov, A. E. Miroshnichenko, D. N. Neshev, A. A. Fedyanin, and Y. S. Kivshar, Multifold enhancement of third-harmonic generation in dielectric nanoparticles driven by magnetic Fano resonances, Nano Lett. **16,** 4857 (2016).

[37] J. Noh, S. Huang, K. P. Chen, and M. C. Rechtsman, Observation of Photonic Topological Valley Hall Edge States, Phys. Rev. Lett. **120,** 063902 (2018).

[38] K. Y. Bliokh, F. Rodríguez-Fortuño, F. Nori, and A. V. Zayats, Spin–orbit interactions of light, Nat. Photonics **9,** 796 (2015).